arXiv:1609.08236v1 [quant-ph] 27 Sep 2016

Resonant transfer of large momenta from finite duration pulse sequences

Julia Fekete[1], Shijie Chai[1], Simon A. Gardiner[2], and Mikkel F. Andersen[1*]
[1] *The Dodd-Walls Centre for Photonic and Quantum Technologies, Department of Physics, University of Otago, Dunedin, New Zealand*
[2] *Joint Quantum Centre (JQC) Durham-Newcastle, Department of Physics, Durham University, Durham DH1 3LE, United Kingdom*

We experimentally investigate the atom optics kicked particle at quantum resonance using finite duration kicks. Even though the underlying process is quantum interference it can be well described by an ϵ-pseudoclassical model. The ϵ-pseudoclassical model agrees well with our experiments for a wide range of parameters. We investigate the parameters yielding maximal momentum transfer to the atoms and find that this occurs in the regime where neither the short pulse approximation nor the Bragg condition is valid. Nonetheless, the momentum transferred to the atoms can be predicted using a simple scaling law, which provides a powerful tool for choosing optimal experimental parameters. We demonstrate this in a measurement of the Talbot time (from which h/M can be deduced), in which we coherently split atomic wave-functions into superpositions of momentum states that differ by 200 photon recoils. Our work may provide a convenient way to implement large momentum difference beam splitters in atom interferometers.

The atom optics δ-kicked particle is a paradigmatic system for experimental studies of quantum chaos and classical-quantum correspondence [1–5]. It consists of laser cooled atoms exposed to a periodically pulsed standing wave (SW) laser field, tuned far off-resonant to relevant atomic transitions. A purely *quantum* phenomenon in such systems is the appearance of quantum resonances (QR) which are a result of self-revivals of the atomic wave-function due to the matter-wave Talbot effect [6]. QRs lead to linear / ballistic growth in the RMS momentum imparted to the atoms with the number of SW pulses [1, 7, 8]. The nonlinear dynamics of the δ-kicked particle enables measurements with sub-Fourier precision [9] both in the vicinity [10, 11] and away from QR [12]. In this context, it is very appealing to realize the large momentum transfer (LMT) of QR as a "beam splitter" (BS) in atom interferometry, as the sensitivity of atom interferometers grows with the momentum difference between the arms. This would allow for applications in high precision metrology such as measurements of h/M [22] etc. A number of atom interferometers today use series of low order Bragg diffraction pulses to realize LMT BS [13, 14]. Using QR bears similarities to this approach since it achieves LMT through consecutive low order diffractions. Compared to a single short pulse BS [6, 15] consecutive pulses can yield enhanced momentum transfer to the atoms. Interestingly, the pulse durations we consider are lower by typically two orders of magnitude compared to Bragg pulses [13, 14, 16]. Using QR thereby reduces the interaction with the SW light, which is a potential source of systematic errors, noise, and decoherence in atom interferometers. Thus, QR is a promising approach for implementing LMT beam splitting processes in an interferometer. The δ-kicked particle description is valid when the motion of the atoms can be neglected during the SW pulses (Raman-Nath approximation). In practice the finite pulse duration often needs to be accounted for numerically [1, 8] when comparing experiments to theoretical predictions. Furthermore, for a given SW power the maximal momentum transfer can be achieved when the SW pulse duration violates the Raman-Nath condition [15, 17]. This has motivated the recent development of an ϵ-pseudoclassical model which accounts for the finite pulse duration effects during QR [18]. Here, we provide the first experimental test of the ϵ-pseudoclassical model which is capable of predicting the momentum transfer to a group of atoms from finite duration SW pulses. We find that the model agrees well with our experiments for a surprisingly large range of pulse durations. For relevant parameters the width of the momentum distribution can be predicted using a simple scaling law. This is a powerful tool that allows for easy optimization of experimental parameters. We demonstrate this by a measurement of the Talbot time in which we split atoms into coherent superpositions of momentum states that differ by up to 200 photon recoils. For the regime where our LMT BS is realized, neither the Raman-Nath approximation nor the Bragg condition holds.

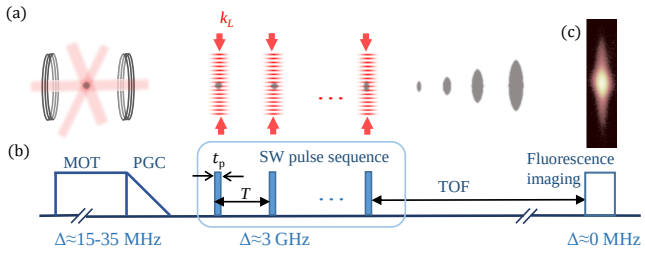

FIG. 1: (Color online) Scheme of the experimental sequence. (a) Laser trapping and cooling; SW pulse sequence; expansion of the atomic cloud during time-of-flight; fluorescence imaging, (b) intensity and detuning (Δ) of light, during the same sequence, not to scale, (c) fluorescence image.

Our experimental sequence consists of the steps depicted schematically in Fig. 1. We trap a cloud of ^{85}Rb atoms in a magneto-optical trap (MOT): subsequent polarization gradient cooling (PGC) leaves the atoms at $\sim$ 6.4 μK in the $|5^2S_{1/2}, F = 2\rangle$ state. We then apply the SW pulse sequence. The SW field is realized by a laser beam retro-reflected from a mirror in the horizontal plane, $\sim$ 40 MHz red detuned from

the $|5^2S_{1/2}, F = 3\rangle \rightarrow |5^2P_{3/2}, F = 4\rangle$ transition. For the initial internal state this light is off-resonant with ~ 3 GHz red detuning. We apply N SW pulses of duration t_p and period T. After the pulse sequence the atomic cloud is let to freely expand for 9.9 ms time-of-flight (TOF), and finally we take a fluorescence image of the atomic distribution. To account for the finite pulse durations we use the ϵ-pseudoclassical model described in [18] (conceptually similar to the approach taken by Wimberger *et al.* [19]). Briefly, the model is as follows. We consider the 1D motion of the atoms along the SW axis. If the kicking period T is an integer multiple (L) of the Talbot time $T_T = 4\pi M/\hbar K^2$ (quantum resonance), then the one period time evolution is governed by the Floquet operator:

$$\hat{F} = \exp\left(-\frac{i}{\hbar}\frac{\hat{p}^2}{2M}[LT_T - t_\mathrm{p}]\right)\exp\left(-\frac{i}{\hbar}\left[\frac{\hat{p}^2}{2M} - \frac{V_\mathrm{d}}{2}\cos(K\hat{x})\right]t_\mathrm{p}\right). \tag{1}$$

The right exponential term is the time evolution during the SW pulse, and the left the free evolution between pulses. M is the atomic mass, and $K = 2k_L$, with k_L the SW laser wave number. $\hat{x}$ and $\hat{p}$ are position and momentum operators, respectively, and V_d is the SW potential depth.

We rewrite the Floquet operator in Eq. (1), taking advantage of two properties. Firstly, due to the spatial periodicity of the SW potential the quasimomentum is conserved, so we restrict our analysis to manifolds of a given quasimomentum β [20]. Secondly, we use the revivals that a spatially periodic wave-function undergoes after free space evolution for duration T_T [6]. Eq. (1) can be rewritten for each β [18] in terms of rescaled dimensionless quantities $\epsilon = \hbar K^2 t_\mathrm{p}/M$, $\hat{\mathcal{J}} = \hat{p}\epsilon/\hbar K$, $\tilde{V} = V_\mathrm{d} t_\mathrm{p}\epsilon/2\hbar$, and $\hat{\theta} = K\hat{x}$ as

$$\begin{aligned}\hat{F}(\beta) = &\exp\left(-\frac{i}{\epsilon}\left[-\frac{\hat{\mathcal{J}}(\beta)^2}{2} + \hat{\mathcal{J}}(\beta)4\pi L\beta\right]\right)\\ &\times\exp\left(-\frac{i}{\epsilon}\left[\frac{\hat{\mathcal{J}}(\beta)^2}{2} - \tilde{V}\cos(\hat{\theta})\right]\right).\end{aligned} \tag{2}$$

In this form of the Floquet operator new quantities appear at different positions. The role of $\hbar$ is played by ϵ which depends on t_p, as also revealed by the commutation relation, $[\hat{\theta}, \hat{\mathcal{J}}] = i\epsilon$. The apparent duration of both exponential operators is one dimensionless time unit. One often speaks of quantum dynamics converging to classical dynamics in the limit of $\hbar \rightarrow 0$. In the ϵ-pseudoclassical model the dynamics of Eq. (2) is approximated with its classical counterpart assuming $\epsilon \ll 1$. The effective classical dynamics is governed by the *effective classical Hamiltonians* extracted from Eq. (2). These are $H_1 = \mathcal{J}(\beta)^2/2 - \tilde{V}\cos(\theta(\beta))$ and $H_2 = -\mathcal{J}(\beta)^2/2 + \mathcal{J}(\beta)4\pi L\beta$. H_1 still has the form of a pendulum, which is exactly solvable in terms of Jacobi elliptic functions. Solving Hamilton's equations of motion for H_2 yields the following map, which gives θ_2 and $\mathcal{J}_2$ after the evolution under H_2 in terms of θ_1 and $\mathcal{J}_1$ before it:

$$\theta_2(\beta) = \theta_1(\beta) - \mathcal{J}_1(\beta) + 4\pi L\beta, \tag{3a}$$

$$\mathcal{J}_2(\beta) = \mathcal{J}_1(\beta). \tag{3b}$$

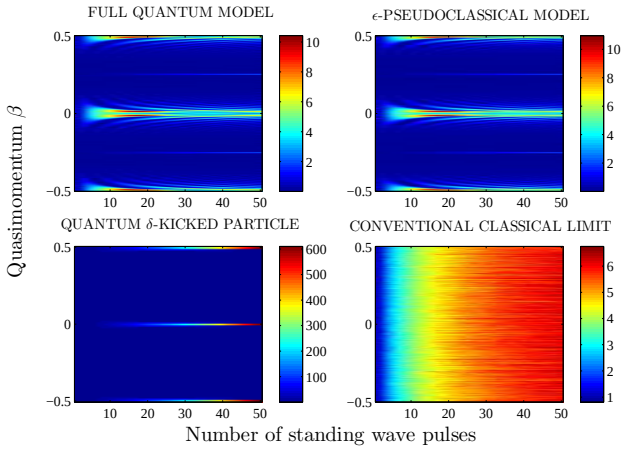

FIG. 2: (Color online) Comparison of $\langle\mathcal{J}^2/2\rangle$ (shown in color coding, see color bars) in different models for $\epsilon = 0.1, \tilde{V} = 1$, as described by Eqs. (1-3).

It is important to note that the ϵ-pseudoclassical model is not the classical limit of our physical system. On the contrary, it consists of mapping the system onto a different classical system that captures the quantum dynamics of the actual system. This is illustrated in Fig. 2 where $\langle\mathcal{J}^2/2\rangle$ (which plays the role of the mean kinetic energy in the ϵ-pseudoclassical model) is plotted as a function of pulse number and initial (quasi-) momentum, computed using different models. For details on the numerical methods see [21]. The ϵ-pseudoclassical model is in quantitative agreement with the full quantum model (Eq. (1)) for the parameters $\epsilon = 0.1, \tilde{V} = 1$ used. Neither the δ-kicked particle model nor the classical model using the Hamiltonians corresponding to the classical limit of Eq. (1) agrees with the full quantum model.

Resonant transfer of kinetic energy to the atoms can be observed close to $\beta = 0$ and to integer multiples of 1/2. It leads to quadratic increase in energy with the number of SW pulses up to a point ($N \approx 5$ pulses in Fig. 2) after which the energy oscillates around a certain value. The strong dependence of QR on β and the limit on the achievable kinetic energy indicates the challenges of transferring large momentum to a finite temperature gas. For the quantum δ-kicked particle the quadratic increase in energy is unlimited, however LMT is not feasible due to the increase of the required laser power with N. H_1, H_2, and Eq. (3) provide insight into the advantage of using consecutive finite duration pulses. For a single pulse the transferred kinetic energy is bounded by the SW potential depth. This can be directly seen from the pendulum Hamiltonian H_1: when the particle reaches the bottom of the potential it will start losing energy again by climbing the next hill. Considering the $\beta = 0$ subspace and Eq. (3) we see that the evolution governed by H_2 does not change the scaled momentum $\mathcal{J}$ (and therefore not the actual momentum) but it changes the position in opposite direction to the momentum. This means that after the particle has rolled down a hill, picking up kinetic energy, the free space evolution by H_2 may bring it back up the hill,

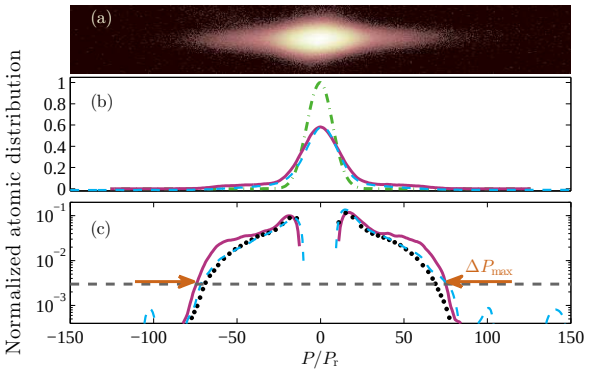

FIG. 3: (Color online) Comparison of experiments and the ϵ-pseudoclassical model for $N = 6, t_p = 250$ ns and $V_d/h = 7.24$ MHz. (a) Average of 10 fluorescence images with logarithmic color map used for calculating momentum distributions. (b) Measured and smoothed momentum distribution without (dash-dotted line) and with SW pulse sequence (dashed line), and ϵ-pseudoclassical model for the same parameters (solid line). (c) Difference curves (SW − no SW). Dashed line is measured data, solid line is from the model and dotted line is from the model including a range of potential depths seen by the atoms.

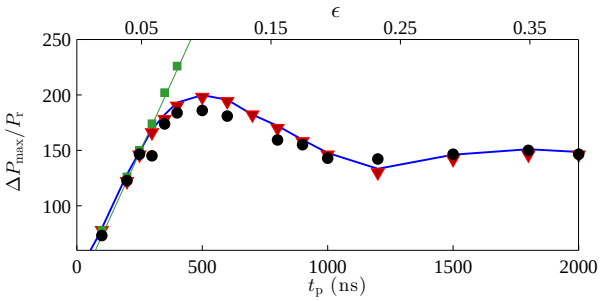

FIG. 4: (Color online) $\Delta P_{\max}$ dependence on t_p. Data measured at $N = 6$, $V_d/h = 7.24$ MHz (circles), the quantum δ-kicked particle (squares with linear fit), full quantum model (triangles) and ϵ-pseudoclassical model (thick solid line) for the same parameters.

thereby allowing it to roll down the hill again during the next evolution under H_1, permitting it to pick up more energy and momentum. In this way the particle can gain significant energy by rolling down the same hill many times. The origin of this apparent backwards motion is in the matter-wave Talbot effect. We note that the free space evolution in Eq. (1) is for a duration $LT_T - t_p$. Since a spatially periodic wave-function revives every T_T, evolving for a duration $T_T - t_p$ is equivalent to a free space evolution of t_p backwards in time. In the ϵ-pseudoclassical model this translates to the position changing in the opposite direction of the momentum. Note, that if $\beta \neq 0$, we get additional motion during the free flight ($4\pi L\beta$ term) suppressing the resonance effect.

To compare measured data with the ϵ-pseudoclassical model, we investigate the cross-sectional atomic distributions along the SW beam axis obtained from averaging 10 repetitions of the experimental sequence (see Fig. 3 as an example). The cross-sectional distributions in the case of no SW light and of a sequence of $N = 6$ pulses are plotted (dash-dotted and dashed lines, respectively) for parameters $t_p = 250$ ns, $V_d/h = 7.24$ MHz and $L = 1$. The total time in the two cases was the same. We deduce the momentum, in units of photon recoil momentum ($P_r = \hbar k_L$), from the images using the time-of-flight. The atomic distributions are broadened due to the SW kicks and a fraction of atoms undergo LMT. To observe the distribution at the wings more carefully, we subtract the distribution with no SW pulses. This difference is shown in Fig. 3 (c) in logarithmic scale after smoothing (dashed line). We determine the maximum momentum difference of the atomic distribution, $\Delta P_{\max}$ at a universal threshold value, indicated with the horizontal dashed line in Fig. 3 (c). The threshold value is chosen to be above the measurement noise level of the smoothed curves and it is a fixed value for all of our measurements. Solid lines in Fig. 3 are calculations with the ϵ-pseudoclassical model. For these calculations the initial width of the atomic distribution and V_d were chosen as best fit parameters, and they are within 25% of the estimated value determined using measured quantities (see details in [21]). The ϵ-pseudoclassical model proved to be a great tool to understand various effects that may come into play during the LMT process. Due to the flexibility of the Monte-Carlo simulations we could easily include various effects that imitate possible physical processes that atoms undergo during their interaction with the SW light sequence without a significant increase in the computational time. Such effects are random phase fluctuations of the SW field or spontaneous photon scattering which result in incoherent momentum exchange. We have also included the effect of non-uniform potential depth over the atomic cloud, which we found to be the dominant effect for the small deviation observed in the upper part of the shoulders in Fig. 3 (c), see [21] for details. Including these variations yielded only a small difference in $\Delta P_{\max}$, therefore we omit them in the following. In Fig. 4 we compare $\Delta P_{\max}$ values calculated with the ϵ-pseudoclassical model, the full quantum model, and the δ-kicked particle model, to experimental data. We plot $\Delta P_{\max}$ values for a series of pulse durations t_p, with $V_d/h = 7.24$ MHz and $N = 6$. The experimental data (circles) are in good agreement with the ϵ-pseudoclassical (thick solid line) and full quantum models (triangles). Here, the range up to $\epsilon \approx 0.39$ ($t_p = 2\ \mu$s) is shown, but the agreement holds up to $\epsilon \approx 1$. This is surprising, as $\epsilon \ll 1$ was assumed for the ϵ-pseudoclassical model to be valid. In contrast, the δ-kicked particle model (squares with linear fit) that predicts linear growth deviates significantly for $t_p > 250$ ns. It should be noted that, when t_p, V_d, and N are large, we observed significant discrepancies between the experimental data and the models. This could be due to phase instability of the SW.

For the $\beta = 0$ subspace, [18] found that $\langle \mathcal{J}^2/2 \rangle$ followed a universal curve if the horizontal axis was scaled appropriately. The general form of this scaling law includes variations in V_d as shown in the inset of Fig. 5. We wish to verify this scaling law experimentally. Since we use a thermal gas, a

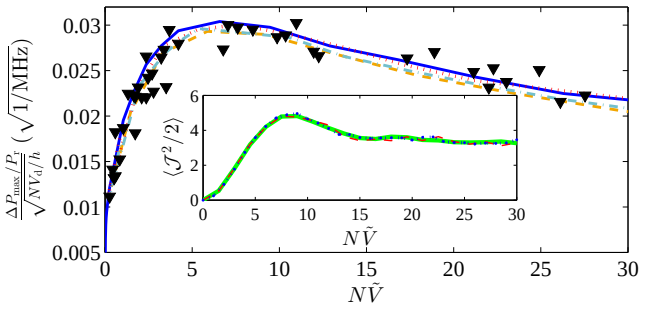

FIG. 5: (Color online) Scaling law. The lines show calculations from the ϵ-pseudoclassical model with t_p scanned at $N = 6, V_d/h =$ 7.24 MHz (solid line), $N = 9, V_d/h = 6.64$ MHz (dashed line), $N = 10, V_d/h = 3.47$ MHz (dotted line), $N = 14, V_d/h = 2.57$ MHz (dash-dotted line). Triangles show measured data within the range of $N = 5 - 12$ and $V_d/h = 2.26 - 7.24$ MHz. Inset shows scaling law for $\langle \mathcal{J}^2/2 \rangle$ with $N = 10, 50, 100$, and $V_d/h = 18.5, 3.7, 0.62$ MHz, respectively for $\beta = 0$.

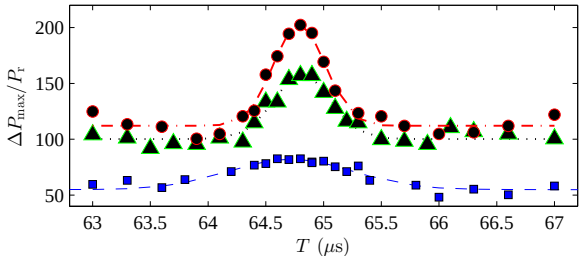

FIG. 6: (Color online) Measurement of the Talbot time. Optimum performance is at $t_p = 430$ ns (circles and dashed line as a guide for the eye). Squares and triangles were measured at $t_p = 180$ and 650 ns, respectively.

measurement of the mean kinetic energy or $\langle \mathcal{J}^2/2 \rangle$ would be skewed by the large proportion of atoms with β away from resonances. However, for a wide range of parameters ΔP_{max} is dominated by the resonant atoms, so it is intriguing to investigate if an equivalent scaling law exists for ΔP_{max}. Fig. 5 shows an equivalent scaled graph for ΔP_{max} assuming that $\langle \mathcal{J}^2/2 \rangle$ of the $\beta = 0$ subspace is proportional to ΔP_{max}^2. The scaling law is transformed (see [21] for details) to make the vertical axis independent of t_p, such that we can use Fig. 5 to determine the optimal value of t_p. We find that, for the parameters chosen, ϵ-pseudoclassical calculations and experimental data approximately follow a universal curve. If one chooses parameters such that ΔP_{max} is not determined by the resonant atoms (e. g. when the characteristic shoulder in Fig. 3 is below our threshold line), then we naturally see deviations from the universal curve. The scaling law described above provides a powerful tool for choosing optimal parameters for experiments using QR. To illustrate this we carry out experiments to observe the resonant transfer of momentum to the atoms as T is scanned across T_T. For chosen values of $N = 10$ and $V_d/h = 5.89$ MHz, the scaling law predicts that the largest ΔP_{max} on resonance is achieved for $t_p \sim 430$ ns. Fig. 6 shows measured data with these parameters. For comparison, data at other values of t_p are also plotted (180 and 650 ns). We see that the largest momentum transfer as well as highest (relative to its baseline) and narrowest peak occur at $t_p = 430$ ns, as expected. From a measured Talbot time ($T_T = 64.8$ μs) one can deduce h/M, where h is Planck's constant. High precision determination of h/M is of general interest, as together with other well known constants it constitutes a measurement of the fine structure constant [22].

The maximum momentum difference of the atomic distribution measured at resonance in Fig. 6 is $\Delta P_{max} = 202\hbar k_L$. If one uses QR as a BS in an atom interferometer, then ΔP_{max} measures the momentum difference between the interferometer arms. In comparison, the state-of-the-art schemes of LMT BS are typically reaching lower values [13, 23]. It has to be noted, that the measurement in Fig. 6 can be interpreted as an atom interferometer itself since QR is a matter-wave interference effect. We would like to point out that we use short pulses compared to Bragg diffraction schemes, which is beneficial for avoiding incoherent photon scattering events. On the other hand, we use pulse durations above the validity range of the δ-kicked particle approximation. Interestingly [16] found that when operated in the quasi-Bragg regime (using t_p too short to fulfill the Bragg condition), their Bragg based atom interferometer reached highest contrast for T that gives rise to QR.

To conclude, we have shown that with just 10 pulses we can generate momentum differences of around 200 $\hbar k_L$. Using QR with finite duration pulses is therefore a promising scheme for a LMT BS that may be applicable in high precision metrology. Furthermore, we have experimentally verified an ϵ-pseudoclassical model that includes finite pulse duration for the atom optics kicked particle at QR. This model captures the quantum behavior with an effective classical treatment. We have found a practically useful scaling law to predict the momentum separation generated as a function of experimental parameters. Combined with the ϵ-pseudoclassical model this is a powerful tool to choose optimum parameters for atom interferometry based on QR.

We acknowledge support from the NZ-MBIE (contract No. UOOX1402), the Leverhulme Trust (Grant No. RP2013-K-009), and the Royal Society (Grant No. IE110202). We thank I. G. Hughes for useful discussions.

* Electronic address: mikkel.andersen@otago.ac.nz; URL: http://www.physics.otago.ac.nz/nx/mikkel/home-page.html

[1] W. H. Oskay, D. A. Steck, V. Milner, B. G. Klappauf, M. G. Raizen, Opt. Commun. **179**, 137 (2000).
[2] M. B. d'Arcy, R. M. Godun, M. K. Oberthaler, D. Cassettari, G. S. Summy, Phys. Rev. Lett. **87**, 074102 (2001).
[3] S. Wu, A. Tonyushkin, M. G. Prentiss, Phys. Rev. Lett. **103**, 034101 (2009).

[4] A. Ullah, S. K. Ruddell, J. A. Currivan, M. D. Hoogerland, Eur. Phys. J. D **66**, 315 (2012).

[5] G. Summy, S. Wimberger, Phys. Rev. A **93**, 023638 (2016).

[6] L. Deng, E. W. Hagley, J. Denschlag, J. E. Simsarian, M. Edwards, C. W. Clark, K. Helmerson, S. L. Rolston, W. D. Phillips, Phys. Rev. Lett. **83**, 5407 (1999).

[7] C. Ryu, M. F. Andersen, A. Vaziri, M. B. d'Arcy, J. M. Grossman, K. Helmerson, W. D. Phillips, Phys. Rev. Lett. **96**, 160403 (2006).

[8] M. Sadgrove, S. Wimberger, S. Parkins, R. Leonhardt, Phys. Rev. Lett. **94**, 174103 (2005).

[9] D. Cubero, J. Casado-Pascual, F. Renzoni, Phys. Rev. Lett. **112**, 174102 (2014).

[10] I. Talukdar, R. Shrestha, G. S. Summy, Phys. Rev. Lett. **105**, 054103 (2010).

[11] A. Tonyushkin, S. Wu, M. Prentiss, Phys. Rev. A **79**, 051402(R) (2009).

[12] P. Szriftgiser, J. Ringot, D. Delande, J. C. Garreau, Phys. Rev. Lett. **89**, 224101 (2002).

[13] S. W. Chiow, T. Kovachy, H. C. Chien, M. A. Kasevich, Phys. Rev. Lett. **107**, 130403 (2011).

[14] T. Mazzoni, X. Zhang, R. Del Aguila, L. Salvi, N. Poli, G. M. Tino, Phys. Rev. A **92**, 053619 (2015).

[15] M. F. Andersen, T. Sleator, Phys. Rev. Lett. **103**, 070402 (2009).

[16] P. A. Altin, M. T. Johnsson, V. Negnevitsky, G. R. Dennis, R. P. Anderson, J. E. Debs, S. S. Szigeti, K. S. Hardman, S. Bennetts, G. D. McDonald, L. D. Turner, J. D. Close, N. P. Robins, New J. Phys. **15**, 023009 (2013).

[17] B. Daszuta, M. F. Andersen, Phys. Rev. A **86**, 043604 (2012).

[18] B. T. Beswick, I. G. Hughes, S. A. Gardiner, H. P. A. G. Astier, M. F. Andersen, B. Daszuta, arXiv:1604.08108v1, to be published.

[19] S. Wimberger, I. Guarneri,S. Fishman, Phys. Rev. Lett. !**92**, 084102 (2004).

[20] R. Bach, K. Burnett, M. B. d'Arcy, S. A. Gardiner, Phys. Rev. A **71**, 033417 (2005).

[21] See Supplemental Material at [URL] for details on the experimental parameters, on numerical methods, on data analysis and on finding the scaling law for a finite temperature gas.

[22] R. Bouchendira, P. Cladé, S. Guellati-Khélifa, F. Nez, F. Biraben, Phys. Rev. Lett. **106**, 080801 (2011).

[23] H. Müller, S. W. Chiow, Q. Long, S. Herrmann, S. Chu, Phys. Rev. Lett. **100**, 180405 (2008).